Enhancing the antibacterial performance of orthopaedic implant materials by fibre laser surface engineering

Document Version:
Publisher's PDF, also known as Version of record

Queen's University Belfast - Research Portal:
Link to publication record in Queen's University Belfast Research Portal

Take down policy
The Research Portal is Queen's institutional repository that provides access to Queen's research output. Every effort has been made to ensure that content in the Research Portal does not infringe any person's rights, or applicable UK laws. If you discover content in the Research Portal that you believe breaches copyright or violates any law, please contact openaccess@qub.ac.uk.

Full Length Article

Enhancing the antibacterial performance of orthopaedic implant materials by fibre laser surface engineering

Chi-Wai Chan [a],*, Louise Carson [b], Graham C. Smith [c], Alessio Morelli [d], Seunghwan Lee [e]

[a] Bioengineering Research Group, School of Mechanical and Aerospace Engineering, Queen's University Belfast, BT9 5AH, UK
[b] School of Pharmacy, Queen's University Belfast, BT9 7BL, UK
[c] Department of Natural Sciences, University of Chester, Thornton Science Park, Chester, CH2 4NU, UK
[d] Centre for Nanostructured Media (CNM), School of Mathematics and Physics, Queen's University Belfast, BT7 1NN, UK
[e] Department of Mechanical Engineering, Technical University of Denmark, DK-2800, Kgs. Lyngby, Denmark

ARTICLE INFO

ABSTRACT

Implant failure caused by bacterial infection is extremely difficult to treat and usually requires the removal of the infected components. Despite the severe consequence of bacterial infection, research into bacterial infection of orthopaedic implants is still at an early stage compared to the effort on enhancing osseointegration, wear and corrosion resistance of implant materials. In this study, the effects of laser surface treatment on enhancing the antibacterial properties of commercially pure (CP) Ti (Grade 2), Ti6Al4V (Grade 5) and CoCrMo alloy implant materials were studied and compared for the first time. Laser surface treatment was performed by a continuous wave (CW) fibre laser with a near-infrared wavelength of 1064 nm in a nitrogen-containing environment. *Staphylococcus aureus*, commonly implicated in infection associated with orthopaedic implants, was used to investigate the antibacterial properties of the laser-treated surfaces. The surface roughness and topography of the laser-treated materials were analysed by a 2D roughness testing and by AFM. The surface morphologies before and after 24 h of bacterial cell culture were captured by SEM, and bacterial viability was determined using live/dead staining. Surface chemistry was analysed by XPS and surface wettability was measured using the sessile drop method. The findings of this study indicated that the laser-treated CP Ti and Ti6Al4V surfaces exhibited a noticeable reduction in bacterial adhesion and possessed a bactericidal effect. Such properties were attributable to the combined effects of reduced hydrophobicity, thicker and stable oxide films and presence of laser-induced nano-features. No similar antibacterial effect was observed in the laser-treated CoCrMo.

© 2017 Elsevier B.V. All rights reserved.

1. Introduction

As a consequence of the soaring number of trauma cases, e.g. from road accidents and sports injuries, and with an increasingly elderly population, there is a strong global demand for orthopaedic prostheses. A recent market research report indicated that the global orthopaedic implants market was valued at USD 4.3 billion in 2015 [1]. Although significant advancements have been made to improve the osseointegration and mechanical properties of orthopaedic implants in the past two decades, orthopaedic implants are still challenged by failures due to various reasons including aseptic loosening and bacterial infections which contribute to 30% and 16% respectively of total joint revision in the hip and knee [2]. Implant failure caused by bacterial infection is costlier,

time consuming, and more difficult to diagnose than aseptic loosening and usually requires the removal of the infected components [3]. Despite the severe consequence associated with implant failure, research into bacterial infection of orthopaedic implants is still at an early stage compared to the research effort on enhancing osseointegration, and on wear and corrosion resistance.

Bacterial infection is initiated through bacterial adherence to the implant surfaces, followed by bacterial colonization and biofilm formation. A biofilm is a community of microorganisms protected by a self-produced extracellular polymeric substance (EPS) matrix. It has been estimated that 99% of bacteria can exist within a biofilm state [4]. Surfaces of different components of orthopaedic implants such as the femoral stem, head and acetabular cup are designed for different purposes. For example, the stem and acetabular cup (back cup), usually made of a titanium alloy (Ti6Al4V), are designed with a rough texture to encourage osseointegration, while the femoral head, usually made of a cobalt-chromium alloy (CoCrMo), is smooth with the aim of reducing the friction between intercalating compo-

nents. Nevertheless, bacteria can adhere to both rough and smooth surfaces, and to different types of materials. Bacterial adherence and subsequent biofilm development can hamper the performance of the implants, for example by interfering with the process of osseointegration [5]. Furthermore, biofilms are extremely difficult to remove with conventional antimicrobial therapies (e.g. antibiotics) and act as a reservoir of bacteria that can lead to chronic and systemic infection [6]. Therefore, strategies to minimise the chances of initial bacterial adherence to the implant surfaces are crucial to prevent bacterial infection.

Bacterial adherence to a surface is dependent on several inter-related surface properties of materials, such as surface roughness, topography, chemistry and wettability. Bacteria prefer to adhere to a rough surface than a smooth surface [7,8], and to hydrophobic rather than hydrophilic surfaces [9,10], while nano-scale surface features are more effective in reducing bacterial adhesion than micro- and macro-scale features [11,12]. Material chemistry can also influence bacterial colonization of a material surface, for example certain metal ions, e.g. silver (Ag), carbon (C), zinc (Zn), copper (Cu), and some metal oxides/nitrides, e.g., titanium dioxide (TiO_2), zinc oxide (ZnO), tantalum nitride (TaN), titanium nitride (TiN), and zirconium nitride (ZrN) [9] all exhibit intrinsic antibacterial properties.

Strategies to reduce bacterial adherence can generally be classified into coating and non-coating methods. The basic concept of coating methods is to coat the entire implant with the aforementioned antibacterial materials. However, the drawback of using antibacterial materials is the possibility of cytotoxicity to the host cells and tissues. For example, copper is known to display cytotoxicity towards mesenchymal stem cells [2]. Non-coating methods directly modify the surface properties of implants to achieve antibacterial characteristics. These methods include reducing surface hydrophobicity [10], creating surface nano-features [12] and modifying surface chemistry [10,13,14].

Laser surface treatment is emerging as a promising non-coating method to negate bacterial adherence. The advantages of laser technology include high speed, cleanliness, high precision and repeatability, as well as flexibility to modify surfaces in selective areas [15]. Further, laser technology can be used along with three-dimensional (3D) printing technology. The laser-based 3D printing technique of selective laser sintering (SLS) has recently been applied to fabricate bone scaffolds with antibacterial properties [16,17].

Recent successful examples of using laser surface treatment techniques to fabricate antibacterial surfaces for metallic implant materials are reviewed as follows: Gallardo-Moreno et al. [10] used UV irradiation at a wavelength of 258 nm to treat Ti6Al4V alloy. Their results indicate that the physicochemical changes on the UV treated surface caused a reduction in the adhesion rate of *Staphylococcus aureus* and *Staphylococcus epidermidis* cells. Kawano et al. [18] used a UV laser with a wavelength of 365 nm to treat commercially pure (CP) Ti. Their study suggests that exposure of CP Ti to a UV laser can decrease the number of attached *Porphyromonas gingivalis* bacterial cells, this bacterium being an important cause of dental implant infections. They ascribed the antibacterial effect to the decrease of water contact angle and increase of the Anatase phase in the surface layer on treated Ti surface. Gillett et al. [19] employed an excimer laser with a wavelength of 248 nm to surface pattern polyethylene terephthalate (PET). They reported that the surface treatment created micro-scale pits in surface and significantly influenced the distribution and morphology of attached *Escherichia coli* cells. Cunha et al. [5] created nano-features on CP Ti surface using a femtosecond laser with a wavelength of 1030 nm. They found that the nano-topography of the laser-induced features reduced adhesion of *S. aureus* cells, and attributed the effect to

the reduction of contact area in the interface between individual bacterium and the metal substrate.

However, each of the studies above concerned only one particular type of materials (i.e. there was no direct comparison across different materials), and the majority of them used laser radiation in the ultraviolet wavelength range (i.e. less than 400 nm). Studies using near-infrared laser (i.e. 700–1800 nm) for enhancement of antibacterial properties of implant materials are very limited. In the work reported here, laser surface treatment was performed on three commonly-used orthopaedic metallic materials, namely CP Ti (grade 2), Ti6Al4V (grade 5) and CoCrMo using a fibre laser with a near-infrared wavelength of 1064 nm in a nitrogen shielding environment. It is known that TiN forms on the surface when Ti-materials react with high power near-infrared laser in the nitrogen environment. TiN is a highly wear-resistant and biocompatible material [15]. *S. aureus*, the most common organism responsible for orthopaedic surgical site infections [20], was selected as the target bacteria in the study. The objectives of this study are (1) to compare the antibacterial effect of different orthopaedic materials before and after laser-treatment with near-infrared radiation, and (2) to explain the difference in antibacterial performance between treated and untreated surfaces in terms of the surface roughness, topography, chemistry and wettability.

2. Experimental details

2.1. Materials

Three different medical grade metallic materials were used for the laser treatment experiments, namely commercially pure Ti (99.2% pure, Grade 2) and Ti6Al4V (Grade 5), and CoCrMo alloy. They were sourced from Zapp Precision Metals GmbH (Schwerte, Germany). The Grade 2 and Grade 5 titanium materials are labeled as TiG2 and TiG5 hereafter. The samples were in the form of discs 30 mm in diameter and 5 mm in thickness. Before laser treatment, the sample surfaces were ground sequentially with a series of SiC papers from 120 to 400 grits following standard metallography procedures to remove pre-existing oxides and ensure surface homogeneity. The samples were then ultrasonically cleaned in ethanol bath for 10 min, rinsed in distilled water for another 10 min, and finally dried thoroughly in a cold air stream.

2.2. Laser treatment experiments in nitrogen environment

The laser treatment process was performed using an automated continuous wave (CW) 200W fiber laser system (MLS-4030). The laser system was integrated by Micro Lasersystems BV (Driel, The Netherlands) and the fibre laser was manufactured by SPI Lasers UK Ltd (Southampton, UK). The wavelength of the laser was 1064 nm. The samples were irradiated with the laser beam using pre-selected processing parameters of: laser power of 40 W, scanning speed of 25 mm/s (meandered scan with lateral movement of 100 μm in the x direction), stand-off distance of 1.5 mm (laser spot size was measured as 100 μm) and shielding with high purity N_2 at 5 bar [21]. The N_2 gas was delivered coaxially with the laser beam via a standard laser nozzle with outlet diameter of 2 mm. The laser-irradiated area on the disk samples was 18 mm × 18 mm and fully covered by laser tracks with overlapping ratio of about 50% in track width.

2.3. Surface morphology, roughness and topography analysis

The surface morphology of the untreated and laser-treated samples was captured using a scanning electron microscope, SEM (Model 6500F, JEOL, Japan). The surface roughness and topography of the untreated and laser-treated samples were assessed

using a portable roughness gauge (Rugosurf 10G, Tesa Technology) and a commercial atomic force microscope (AFM) in tapping mode (D5000, Veeco Digital Instruments). The surface roughness tester was used to measure the 2D large step surface profiles (in macro-scale) whilst the AFM served to characterize the 3D micro/nano-scale features in local areas of the surface. The scan length of the surface roughness tester was 15 mm whilst the scan size of the AFM was $2 \mu m \times 2 \mu m$. Basic roughness parameters, namely Ra (arithmetic mean roughness) and Rz (maximum height of profile) were measured using the surface roughness tester. At least 12 measurements were taken at different locations for each sample in the direction perpendicular to the laser track orientation. The additional surface roughness parameters, namely Rsk (skewness of profile) and Rku (kurtosis of profile) were measured by AFM. At least two measurements were taken for each sample. The locations of measurements were randomly selected from the untreated surfaces whilst the measurements were taken at the region near the centreline of laser tracks in the laser-treated surfaces. Topographic analysis was performed via the WSxM software [22].

2.4. Surface wettability analysis

The sessile drop method was used to measure the contact angle of a liquid drop on the untreated and laser-treated samples using a video-based contact angle analyzer (FTA 200, First Ten Angstroms). The image capture and analysis were performed using the FTA 32 video software. Deionized water was used as the testing liquid, and the volume of each sessile drop was controlled at 5 μl using a microlitre syringe. Droplet images were captured in the direction perpendicular to the laser track orientation at fixed time intervals, counting since the start of droplet deposition to the cessation of droplet spreading or at least 60 s. At least eight measurements were taken at different locations for each sample at room temperature.

2.5. Surface chemistry analysis

X-ray photoelectron spectroscopy (XPS) spectra were acquired using a bespoke ultra-high vacuum system fitted with a monochromated Al Kα X-ray source (Specs GmbH Focus 500, Berlin) with a photon energy of 1486.6 eV, 150 mm mean radius hemispherical analyser with 9-channeltron detection (Specs GmbH Phoibos 150, Berlin), and a charge neutralising electron gun (Specs GmbH FG20, Berlin). The analysis area was approximately 2 mm in diameter. Survey scans were acquired over the binding energy range between 0 and 1100 eV using a pass energy of 50 eV, and the high-resolution scans over the Ti 2p (for TiG2 and TiG5), Al 2p (for TiG5), Co 2p and Cr 2p (for CoCrMo), and N 1 s (for all types of sample) lines were made using a pass energy of 15 eV. Data were quantified using Scofield cross-sections corrected for the energy dependencies of the effective electron attenuation lengths and the analyser transmission. Data processing and curve fitting were carried out using the CasaXPS software v2.3.16 (CasaXPS, Teignmouth, UK).

2.6. Bacterial cell culture

Both the laser-treated and untreated control samples of TiG2, TiG5 and CoCrMo alloys were used for bacterial adherence and biofilm formation assays. The samples were cut in the form of circular discs with 8 mm diameter by electric discharge machining (EDM). Samples were cleaned with pure ethanol (Sigma Aldrich, UK) in an ultrasonic bath for 15 min prior to bacterial cell culture. The dry, clean samples were then placed into a 24-well tissue culture plate. They were then sterilized with 70% ethanol for 10 min and washed three times with sterile phosphate buffered saline (PBS). *S. aureus* (ATCC 6538) was cultured in Müller Hinton Broth (MHB; Oxoid) overnight (18 h) at 37 °C on a gyrotatory incubator with shaking at 100 rpm. After incubation, sterile MHB was used to adjust the overnight culture to an optical density of 0.3 at 550 nm and diluted 1 in 50 with fresh sterile MHB. This provided a bacterial inoculum of approximately 1×10^6 Colony Forming Units (CFU)/ml. 1 ml of culture was applied to each sample at an inoculum not exceeding 2.4×10^6 CFU/ml, as verified by viable count. The samples were incubated for 24 h at 37 °C on a gyrotatory incubator with shaking at 100 rpm. Three samples of each type of materials, for both untreated and laser-treated, were tested to ensure the consistency of the results.

2.7. Bacterial viability analysis

After 24 h of incubation, the samples were washed three times with sterile PBS to remove any non-adherent bacteria. The adherent bacteria were stained with fluorescent Live/Dead® BacLight™ solution (Molecular Probes) for 30 min at 37 °C in the dark. The fluorescent viability kit contains two components: SYTO 9 dye and propidium iodide. The SYTO 9 labels all bacteria, whereas propidium iodide enters only bacteria with damaged membranes. Green fluorescence indicates viable bacteria with intact cell membranes whilst red fluorescence indicates dead bacteria with damaged membranes. The labelled bacteria were observed using a fluorescence microscope (GXM-L3201 LED, GX Optical). At least ten random fields of view (FOV) were captured per sample. The surface areas covered by the adherent bacteria were calculated using the ImageJ software (developed at the National Institutes of Health, Bethesda, Maryland, U.S.)(https://imagej.nih.gov/ij/). The areas corresponding to the viable bacteria (coloured green) and the dead bacteria (coloured red) were individually calculated. The total biofilm area was the sum of the green and red areas and the dead/live cell ratio was the ratio between the green and red areas. The results were expressed as the means of measurements from the ten images.

2.8. Bacterial morphology analysis

After removing samples from the bacterial culture, the samples were initially rinsed with 0.9% saline for 1 min to remove any non-adherent bacteria. This process was repeated three times. The adherent bacteria were then fixed using 2.5% glutaraldehyde in 0.1 M cacodylic acid (pH 7.2). The samples were kept in this solution for 24 h at 4 °C. After the fixation, the samples were dehydrated in a graded series of ethanol: 50%, 70%, 90% and 100% with 30 min each at room temperature. The dehydrated samples were then transferred to a 24-well plate containing a dying agent of hexamethyldisilazane (HMDS) and left to dry for 24 h in a fume cupboard. The samples were sputter-coated with Au for bacteria morphology observation by SEM (Model 6500F, JEOL, Japan). The clean samples were imaged by SEM as a control.

2.9. Statistical analysis

The significance of the observed differences between the means of different samples were analysed and compared by one-way ANOVA and Tukey's test using SPSS software (version 19, SPSS, Inc.). The probability below $p < 0.05$ was considered as statistically significant.

3. Results

3.1. Surface morphology by SEM

The SEM micrographs for the untreated and laser-treated surfaces are shown in Fig. 1(a–i). A typical surface morphology after mechanical grinding can be observed from the untreated surfaces
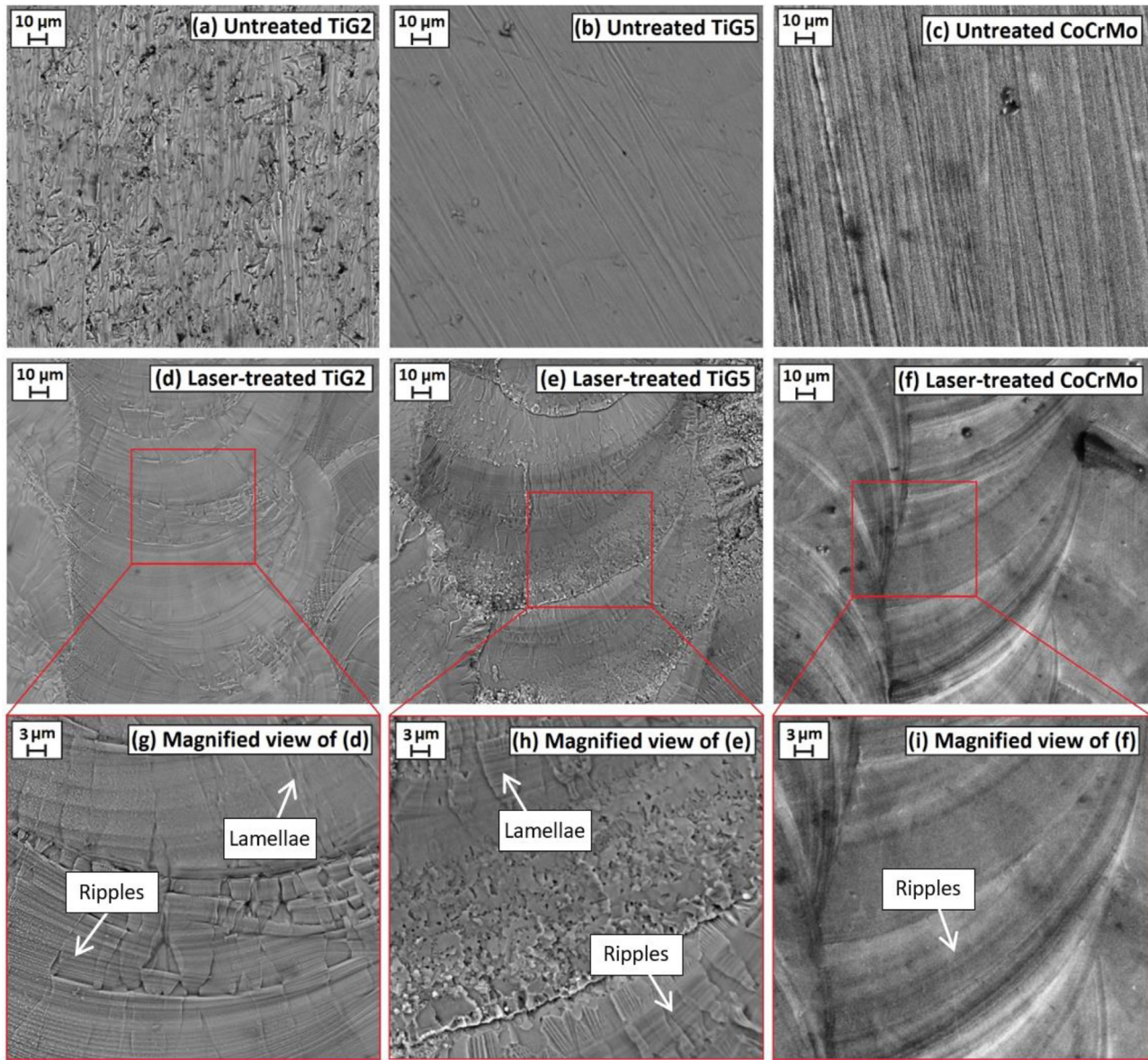
Fig. 1. (a–i). SEM micrographs for the (a–c) untreated and (d–i) laser-treated samples: TiG2 (a, d & g), TiG5 (b, e & h) and CoCrMo (c, f and i). The micrographs from (a) to (f) are at lower magnification of 1000, whilst the micrographs from (g) to (i) are the magnified views of (d) to (f) at 3000.

of TiG2, TiG5 and CoCrMo, showing the presence of randomly-oriented scratch marks (Fig. 1a–c). As observed in Fig. 1d–f, all laser-treated surfaces, namely TiG2, TiG5 and CoCrMo, show circular rosette-like markings. Such rosette-like markings were created as a consequence of the moving laser beam (operated at CW mode) "stopping" at each location on the metal surface for a very short period of time during the laser treatment process, allowing the laser beam to melt and interact with the metal [21]. Using the empirical equation derived by Suder and Williams [23], the interaction time (i.e. laser spot diameter divided by scanning speed) between the laser beam and the metal surface was calculated as 4 ms. The magnified views in Fig. 1g and h show that the rosette-like markings in laser-treated TiG2 and TiG5 surfaces consist of secondary micro-/nano-sized features such as ripples and radial lamellae (see arrows in Fig. 1g and h). The ripple features (see arrow in Fig. 1i) can still be found in the rosette-like markings of laser-treated CoCrMo but radial lamellae are absent from the surface.

3.2. Surface roughness by 2D roughness tester

The Ra and Rz values for the untreated and laser-treated samples extracted from the 2D roughness profiles are given in Table 1. The Ra values for the untreated samples are in the range of 0.04–0.36 μm, while the Rz values are between 0.33 and 2.58 μm. The Ra and Rz values of the untreated samples follow the same order with the untreated TiG2 being the highest, followed by the untreated TiG5 and the lowest is the untreated CoCrMo. Both the Ra and Rz values increase significantly after laser treatment, with the Ra and Rz values lying between 1.82 and 3.56 μm and between 10.85 and 18.70 μm, respectively. However, the order is different from that which is observed in the group of the untreated samples, with the laser-treated TiG5 being the highest, followed by the laser-treated TiG2 and the lowest is the laser-treated CoCrMo. It can be observed that the TiG2 and TiG5 samples in the untreated and laser-treated groups have higher Ra and Rz values than the CoCrMo sample.

Table 1
Summary of the surface roughness parameters and water contact angles for the untreated and laser-treated samples: TiG2, TiG5 and CoCrMo.

| Samples	Surface Roughness Parameters				Surface Wettability
	Ra (µm) Measured by 2D Surface Roughness Tester	Rz (µm)	Rsk Measured by AFM	Rku	Water Contact Angle (°) Measured by SessileDrop Method
Untreated TiG2	0.37	2.59	−0.34	2.06	74.3
Untreated TiG5	0.13	1.14	0.22	2.29	72.6
Untreated CoCrMo	0.04	0.33			80.6
Laser-treated TiG2	2.60	18.70	0.07	3.04	31.9
Laser-treated TiG5	3.57	23.23	0.32	3.11	45.7
Laser-treated CoCrMo	1.83	10.86			83.0
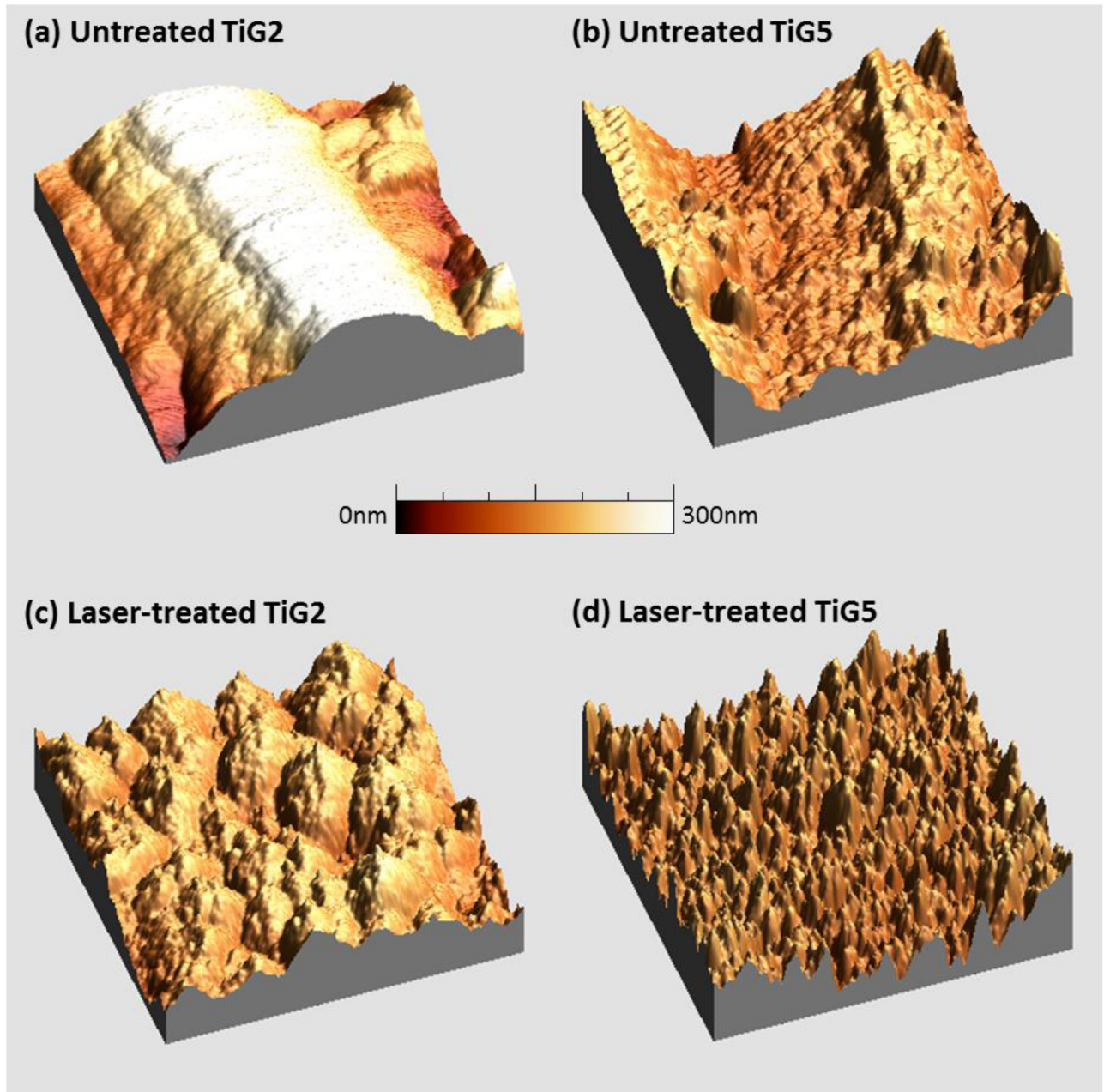
Fig. 2. (a–d). AFM topography 3D images for the (a-b) untreated and (c-d) laser-treated TiG2 and TiG5. Scan area $2 \times 2\,\mu m^2$; color coding of all images as by height scale in figure.

3.3. Surface topography by AFM

The secondary surface features in the laser-treated TiG2 and TiG5 (refer to Fig. 1g and h) were further analysed using AFM. The untreated TiG2 and TiG5 surfaces were used as control. The secondary surface features were quantified by two additional surface roughness parameters, namely Rsk and Rku. The Rsk and Rku values for the untreated and laser-treated TiG2 and TiG5 are given in
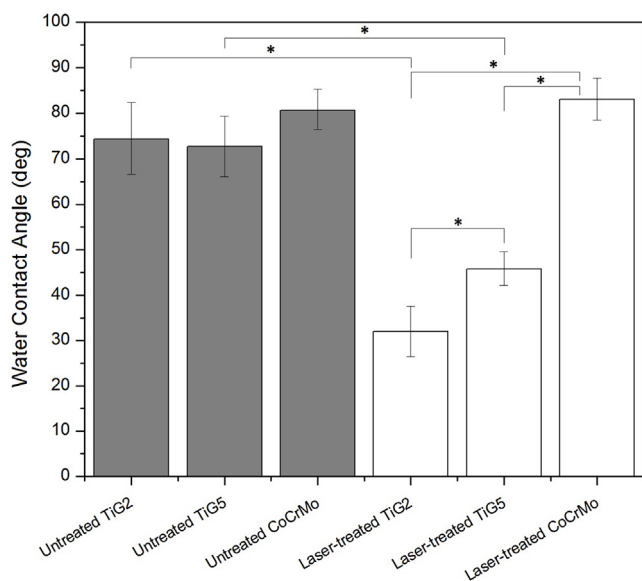
Fig. 3. Mean contact angles of water (n = 8) with error bars (95% confident interval) for the two groups of samples: untreated and laser-treated samples. Within the group of the untreated samples, no significant differences are observed. Within the group of the laser-treated samples, the laser-treated CoCrMo has the highest contact angle, followed by the laser-treated TiG5 and the laser-treated TiG2 has the lowest. Results are statistically significant at p < 0.05. A statistically significant reduction in the contact angle is observed in the laser-treated TiG2 and TiG5 when comparing with their untreated counterparts. No statistically significant difference exists between the untreated and laser-treated CrCrMo. *indicates the mean difference is significant at p < 0.05.

Table 1, and their 3D surface profiles are provided in Fig. 2(a–d). Rku is a measure of the sharpness of the profile. Spiky surfaces have a high kurtosis value (Rku > 3) whereas bumpy surfaces have a low kurtosis value (Rku <3). Rsk describes the asymmetry of a surface. A negative skewness value indicates a predominance of troughs whereas a positive skewness value indicates an abundance of peaks.

The results in Table 1 indicate that untreated TiG2 and TiG5 have a low Rku value (<3) but TiG2 has a negative Rsk whilst TiG5 has a positive Rsk. In comparison, both the laser-treated TiG2 and TiG5 have a positive Rsk and a high Rku (>3). The results of skewness and kurtosis analysis point to the fact that both untreated TiG2 and TiG5 tend to have a bumpy surface (Fig. 2a and b) but untreated TiG2 has more troughs than peaks though the opposite is found in untreated TiG5. Laser-treated TiG2 and TiG5 tend to have a spiky surface (Fig. 2c and d) with more peaks than troughs in the surface, i.e. due to the presence of secondary surface features. As seen in Fig. 2c and d, the secondary surface features on laser-treated TiG5 are noticeably smaller and spikier than those on laser-treated TiG2.

3.4. Surface wettability by sessile drop method

The water contact angles on the untreated and laser-treated samples are given in Table 1 and plotted in Fig. 3. It has been reported that material surfaces can be considered hydrophobic if the water contact angle is larger than 50° [24]. From the results in Table 1, all untreated samples have a high contact angle of over 70°, indicating that untreated TiG2, TiG5 and CoCrMo are hydrophobic. On the other hand, the water contact angles on laser-treated TiG2 and TiG5 are found to be remarkably smaller, with statistical significance (p < 0.05). This indicates that the surface hydrophobicity of TiG2 and TiG5 is greatly reduced after laser treatment. Furthermore, the decrease in the contact angle is more profound for laser-treated TiG2 than laser-treated TiG5. The contact angle on untreated and

laser-treated CoCrMo is similar to each other. The order of surface hydrophobicity for the laser-treated samples is:
Laser-treated CoCrMo > Laser-treated TiG5 > Laser-treated TiG2.

3.5. XPS survey scans

The surface composition results in atom%, excluding H and He, and normalised to 100% of elements detected, are shown in Table 2. A number of observations can be made from the survey scan results. Comparing results for TiG2 and TiG5, the levels of Ti are reduced by laser treatment, slightly in the case of TiG2 and by more than half in the case of TiG5. In both materials, surface oxygen levels are reduced but nitrogen levels are increased after laser treatment. This suggests that the native surface oxide was replaced by a second surface film (e.g. TiN) during laser treatment. Carbon is present on the untreated and laser-treated samples in the form of adventitious hydrocarbon, i.e. residual contamination. Additionally, TiG5 shows Al and V on the untreated surface. However, the surface ratio of Ti, Al and V is far from that of the bulk composition, indicating surface enrichment in Al. After laser treatment, this surface enrichment is even more pronounced, with considerably more Al than Ti at the surface. It is particular noteworthy that no V is detected from laser-treated TiG5. As for CoCrMo, both untreated and laser-treated surfaces show high levels of carbon. The levels of Co and Cr are slightly increased after laser-treatment. However, the Co and Cr levels are rather low in both surfaces, probably as a result of attenuation of the signal by the hydrocarbon overlayer. The oxygen levels are increased with laser treatment, as are the levels of Cr and Co. Nevertheless, no increase is found in the nitrogen levels after laser treatment.

3.5.1. Narrow scan of N 1 s spectrum (for TiG2, TiG5 and CoCrMo)
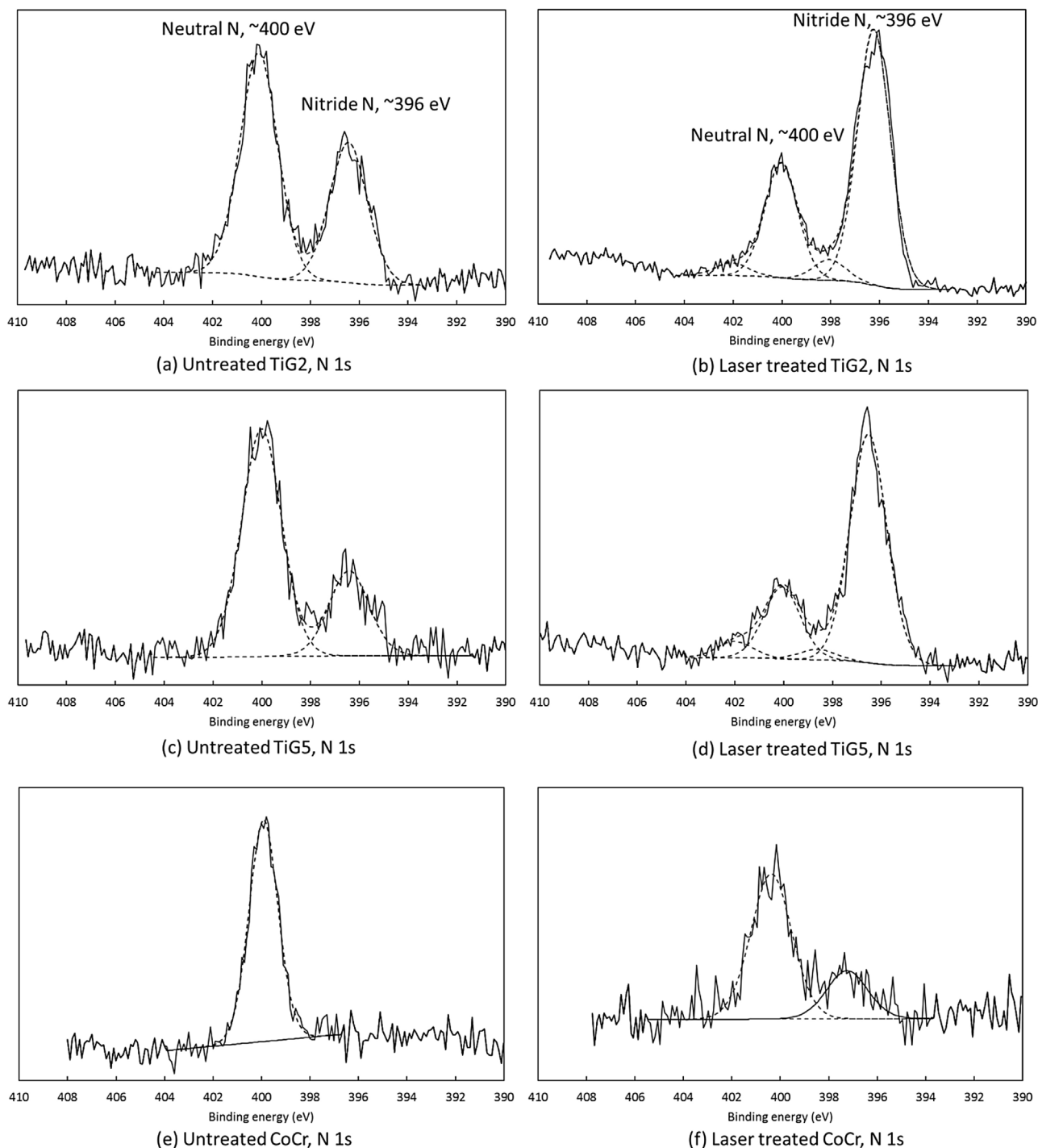
High resolution scans over the N 1 s line on the untreated and laser-treated surfaces of TiG2, TiG5 and CoCrMo are shown in Fig. 4(a–f). Two peaks are seen from TiG2 (Fig. 4a and b) and TiG5 (Fig. 4c and d). The component at 396 eV is due to nitrogen in the form of nitride; that at 400 eV is due to nitrogen in an electronically neutral form typical of an organic species (e.g. amine-type bonding) and is attributed to the general low-level environmental contamination expected on air-exposed surfaces. Comparing untreated and laser-treated TiG2, the results indicate a substantial increase in the nitride component on laser-treated TiG2 (Fig. 4b) and this increase in the nitride component accounts for the increase in the total nitrogen level from 3.9% to 7.7% shown in Table 2. Likewise, a substantial increase in the relative proportion of the nitride component is observed on laser-treated TiG5 (Fig. 4d) but the increase in the total amount of nitrogen from 2.7% to 3.6% is not as great as seen for laser-treated TiG2 (Table 2). Regarding CoCrMo (Fig. 4e and f), only one peak at 400 eV is seen on the untreated sample (Fig. 4e). On laser-treated CoCrMo (Fig. 4f), the N 1 s spectrum shows the presence of a further component at 397 eV, an energy typical of a metal nitride form. However, the proportion of the nitride component is very small, and thus there is not enough evidence to support the existence of a significant nitride film on laser-treated CoCrMo.

3.5.2. Narrow scan of Ti 2p spectrum (for TiG2 and TiG5)

The Ti 2p spectra from the untreated and laser-treated surfaces of TiG2 and TiG5 are shown in Fig. 5(a–d). Each chemically-shifted Ti 2p peak is split into $2p_{3/2}$ and $2p_{1/2}$ doublets. The various chemically-shifted components of the Ti $2p_{3/2}$ peak are found as follows: Ti^0 or metallic Ti = 454 eV, TiO = 455 eV, TiN or Ti_2O_3 = 455.8 eV and TiO_2 = 458.8 eV. The spectrum from the untreated TiG2 surface (Fig. 5a) is dominated by a strong TiO_2 component, as expected for an air-exposed Ti surface. Metallic Ti is visible, indicating that the surface oxide film is probably very thin (~few nm). Low levels of intermediate states including TiO and

Table 2
Summary of atom% compositions by XPS on the untreated and laser treated samples: TiG2, TiG5 and CoCrMo.

Elements & lines	TiG2		TiG5		CoCrMo	
	Untreated	Laser-treated	Untreated	Laser-treated	Untreated	Laser-treated
Ti 2p	9.0	8.1	3.8	1.5	––	––
Al 2p	––	––	5.4	12.5	––	––
V 2p3/2	––	––	0.2	––	––	––
Co 2p3/2	––	––	––	––	1.8	2.7
Cr 2p3/2	––	––	––	––	1.6	2.6
O 1s	32.8	28.0	23.3	23.0	13.1	19.6
N 1s	3.9	7.7	2.7	3.6	2.9	1.7
C 1s	50.1	53.7	62.1	55.6	80.7	72.0
Others: Ca 2p, Cl 2p, Fe 2p, P 2s, S 2p, Si 2p, Zn 2p3/2	4.3	2.5	2.5	3.8	0.0	1.5

(a) Untreated TiG2, N 1s

(b) Laser treated TiG2, N 1s

(c) Untreated TiG5, N 1s

(d) Laser treated TiG5, N 1s

(e) Untreated CoCr, N 1s

(f) Laser treated CoCr, N 1s

Fig. 4. (a-f). XPS N 1 s spectra from the untreated and laser-treated samples:.   (a–b) TiG2–N 1s, (c–d) TiG5–N 1 s and (e-f) CoCrMo–N 1s
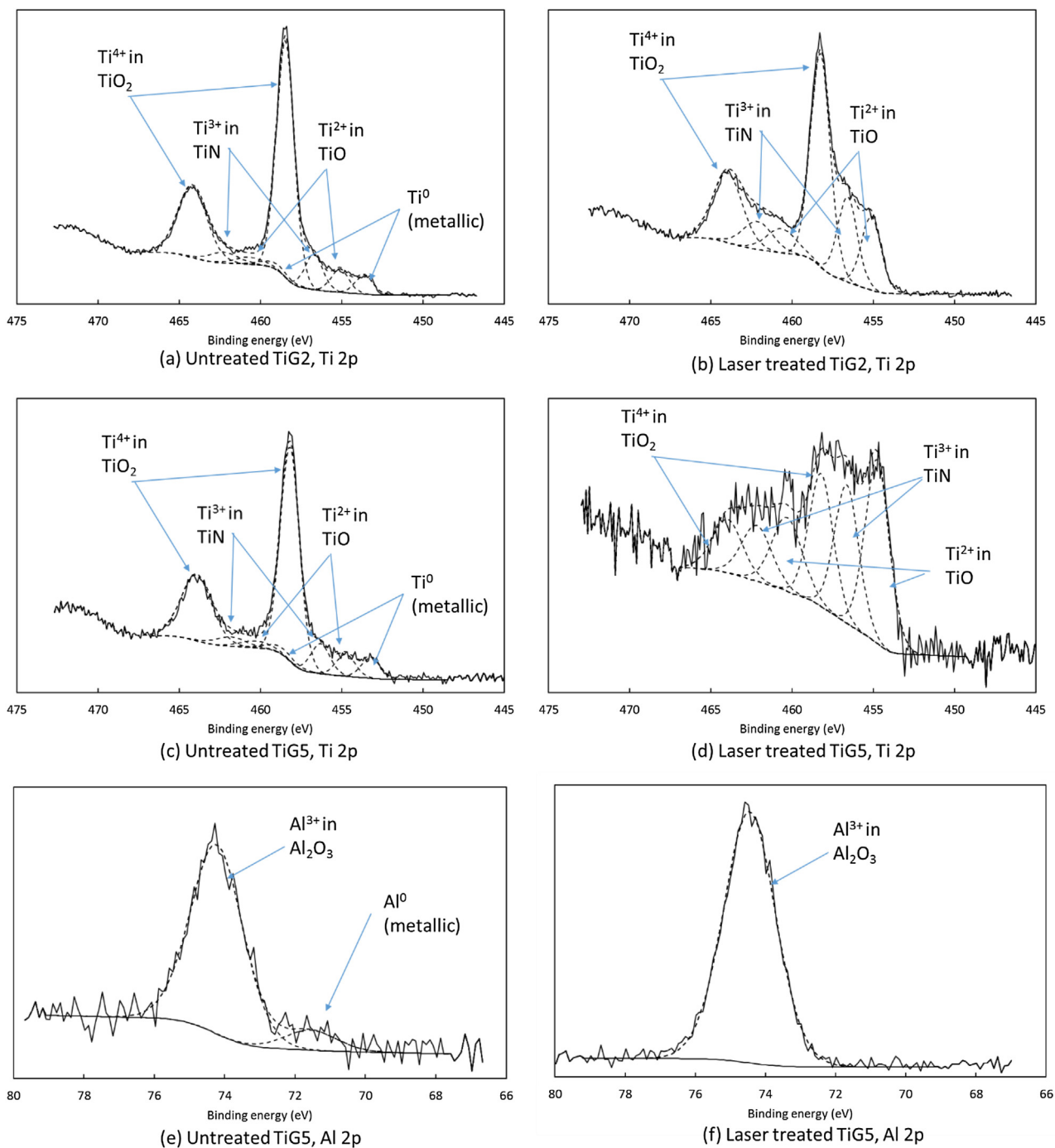
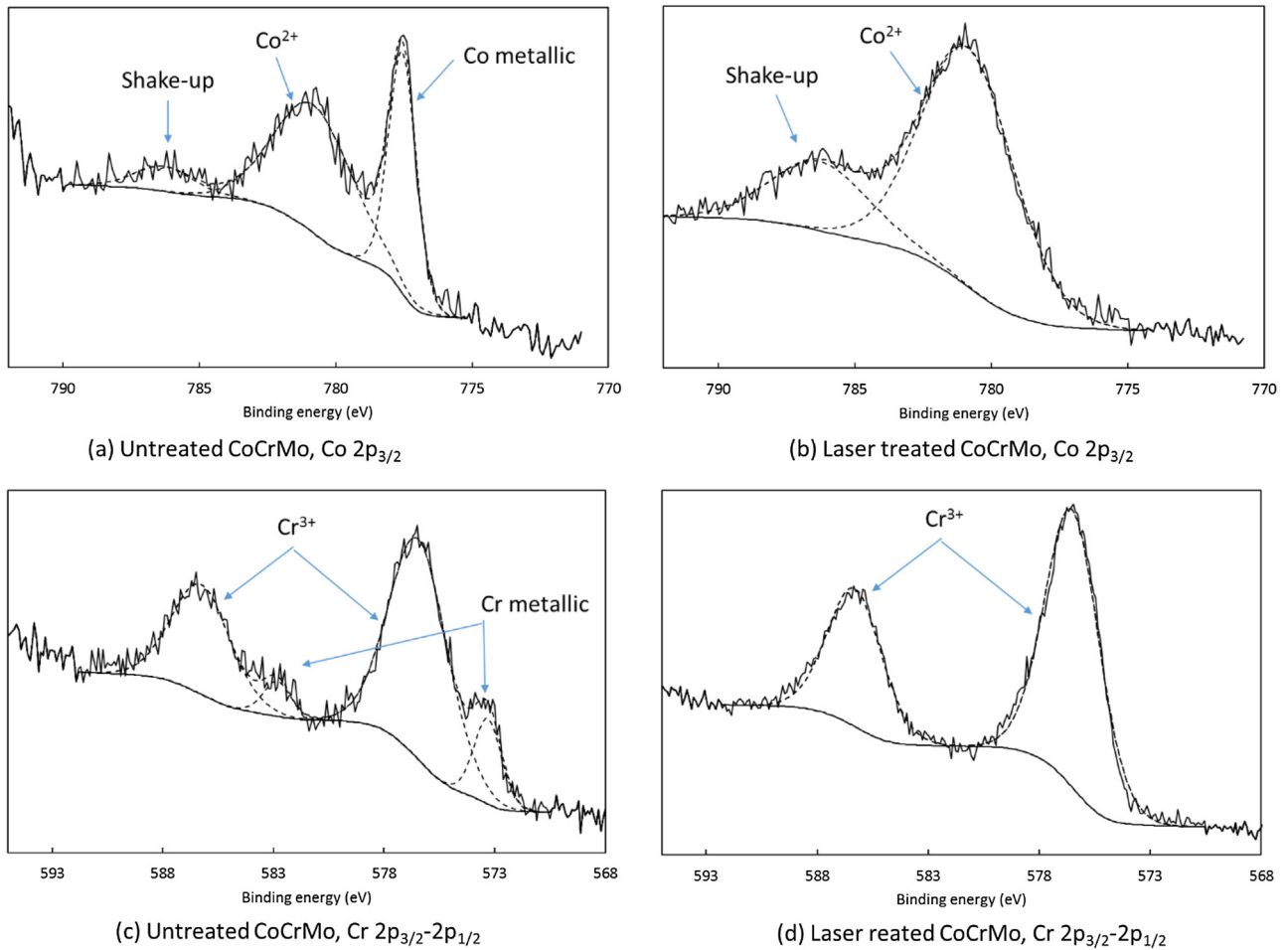**Fig. 5.** (a-f). XPS Ti 2p and Al 2p spectra from the untreated and laser-treated samples:.   (a-b) TiG2–Ti 2p, (c-d) TiG5–Ti 2p and (e-f) TiG5–Al 2p

TiN/Ti_2O_3 are also visible. After laser treatment, the spectrum of TiG2 (Fig. 5b) shows no metallic Ti. As a proportion of the total Ti signal, the TiO_2 component is lower and the TiN and TiO components are stronger than were found on untreated TiG2. On TiG5, the spectrum of the untreated surface (Fig. 5c) looks very similar to that from the equivalent area of untreated TiG2. The Ti 2p region is dominated by strong TiO_2 components, and low levels of Ti metal, Ti^{2+} and Ti^{3+} are also detected. The Ti^{3+} component has been attributed to TiN, as nitride is seen in the N 1 s spectra, but Ti_2O_3 or some mixed oxy-nitride component cannot be ruled out from these data. On the laser-treated TiG5 surface (Fig. 5d), the spectrum shows no metallic component, as is the case for laser-treated TiG2. However,

the TiO_2 component after laser treatment is considerably weaker than that in the laser-treated TiG2.

3.5.3. Narrow scan of Al 2p spectrum (for TiG5 only)

The Al 2p spectra from untreated and laser-treated TiG5 surfaces are shown in Fig. 5(e–f). On both untreated and laser-treated surfaces, the spectra are dominated by major components at approximately 74.2–74.4 eV, corresponding to Al in its highest oxidation state, Al_2O_3 or possibly $Al(OH)_3$. On the untreated TiG5 (Fig. 5e), there is some evidence for a weak component at approximately 71.6 eV corresponding to Al in a metallic alloy form. On the laser-treated TiG5 (Fig. 5f), the effect of the laser treatment appears to have been to convert a thin oxide film where some

(a) Untreated CoCrMo, Co $2p_{3/2}$

(b) Laser treated CoCrMo, Co $2p_{3/2}$

(c) Untreated CoCrMo, Cr $2p_{3/2}$-$2p_{1/2}$

(d) Laser reated CoCrMo, Cr $2p_{3/2}$-$2p_{1/2}$

Fig. 6. (a–d). XPS Co 2p and Cr 2p spectra from the untreated and laser-treated samples:. (a-b) CoCrMo–Co 2p, and (c-d) CoCrMo–Cr 2p

metallic character could be detected, into a fully formed oxide. In this case, a substantial increase in the amount of Al at the surface is also detected, possibly indicating migration or segregation to the surface and subsequent oxidation as a consequence of the laser treatment.

3.5.4. Narrow scan of Co 2p and Cr 2p spectrum (for CoCrMo only)

The Co 2p and Cr 2p spectra from the untreated and laser-treated CoCrMo surfaces are shown in Fig. 6(a–d). The Co spectral range (Fig. 6a and b) shows a doublet consisting of $2p_{3/2}$ components in the binding energy range 775–790 eV and $2p_{1/2}$ components in the energy range 791–808 eV. The Co $2p_{3/2}$ spectral region from the untreated surface (Fig. 6a) shows a sharp and relatively intense component at 778 eV and a broad feature at 781 eV. The sharp feature at 778 eV is due to the metallic Co and the feature at 781 eV is due to oxidised Co in the form of CoO. On the laser treated surface (Fig. 6b), there is no evidence for metallic Co. The Co appears fully oxidised in the Co^{2+} form. Furthermore, the Cr 2p spectra (Fig. 6c and d) mirror the behaviour of the Co 2p. On the untreated surface (Fig. 6c), the spectrum shows the metallic Cr and the oxidised Cr in the form of Cr_2O_3. On the laser-treated surface (Fig. 6d), only the oxide components are seen, i.e. no evidence for the metallic Cr.

3.6. Fluorescence images (Live/Dead staining) of biofilms

The images obtained by fluorescence microscopy in Fig. 7 (a–e) shows the adhesion of S. aureus on the untreated (Fig. 7a, c and e) and laser-treated (Fig. 7b, d,and f) surfaces after 24 h culture. The green and red colours indicate the bacterial cells with intact (live) and damaged membrane (dead), respectively. As seen in the figures, a high amount of green fluorescence is found from the surfaces of all untreated samples, namely TiG2 (Fig. 7a), TiG5 (Fig. 7c) and CoCrMo (Fig. 7e), indicating a high number of viable bacterial cells adhered on the surfaces. The viable cells are able to adhere and grow on the untreated surfaces and aggregate to form the biofilms. In comparison, the number of viable bacteria on the laser-treated TiG2 is reduced remarkably (Fig. 7b), i.e. only a small amount of green fluorescence is evident. In addition to the reduced number of viable cells, red staining (non-viable bacteria) is dominant on the laser-treated TiG2. Similar observations are seen on the laser-treated TiG5 (Fig. 7d). These findings indicate that the laser-treated TiG2 and TiG5 surfaces may be less hospitable for S. aureus adherence and may possess a bactericidal effect. In contrast, green-fluorescence from viable bacteria was dominant on the laser-treated CoCrMo surface (Fig. 7f).

3.7. Statistical analysis of bacterial adhesion and bactericidal effect

The bacterial adhesion is quantified by calculating the percent of total biofilm area. The results are plotted in Fig. 8. The results show that the laser-treated TiG2 and TiG5 surfaces exhibited a noticeable reduction in bacterial adhesion when compared to their untreated counterparts. The results are statistically significant at $p < 0.05$. However, there was no statistically significant difference between the untreated and laser-treated CoCrMo in bacterial adhesion. The
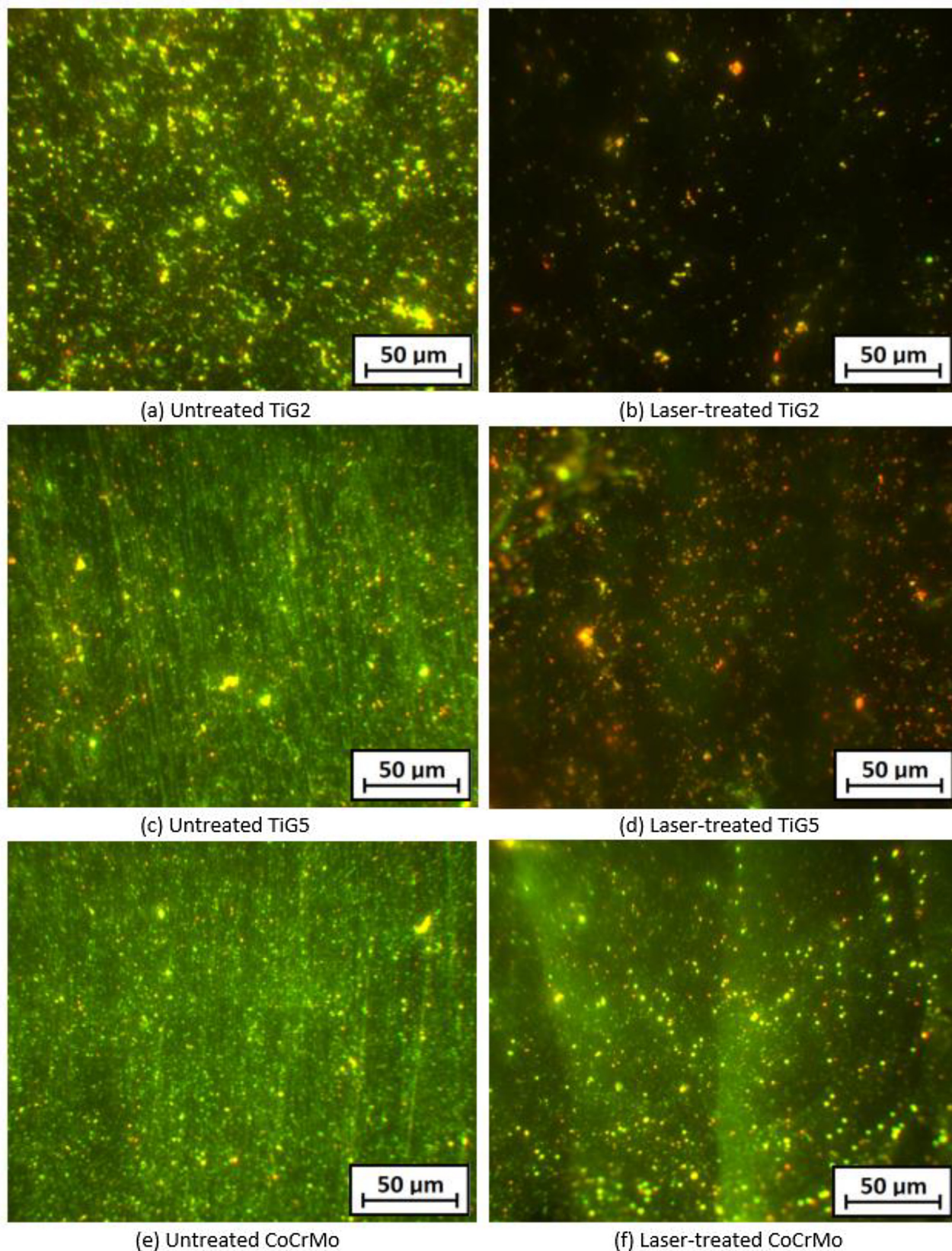
Fig. 7. (a–f). Fluorescence images for the untreated and laser-treated samples after 24 h of bacterial cell culture: TiG2 (a and b), TiG5 (c and d) and CoCrMo (e and f).

order of ability to reduce the bacterial adhesion is laser-treated TiG2 > laser-treated TiG5 > laser-treated CoCrMo ($p < 0.05$). On the other hand, the bactericidal effect is quantified by calculating the dead/live cell ratio for each surface, i.e. the higher the ratio, the more efficacious the bactericidal effect. The results are plotted in Fig. 9. The results show that the laser-treated TiG2 and TiG5 have
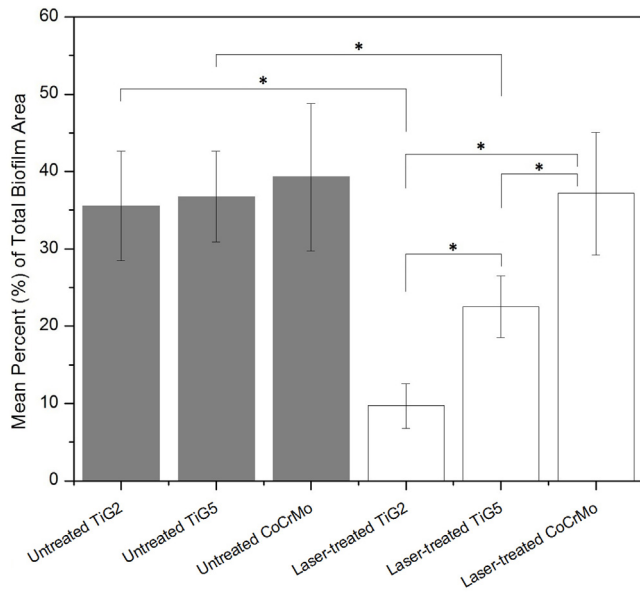
Fig. 8. Mean percent (%) of total biofilm area (n = 10) with error bars (95% confident interval) for the two groups of samples: untreated and laser-treated samples. Within the group of untreated samples, no significant differences are observed. Within the group of laser-treated samples, the laser-treated CoCrMo shows the highest percent of total biofilm area, followed by the laser-treated TiG5 and the least is the laser-treated TiG2. Results are statistically significant at p < 0.05. Comparing between the untreated and laser-treated samples, a statistically significant reduction (p < 0.05) are observed with the laser-treated TiG2 and TiG5, respectively. No significant differences exist between the untreated and laser-treated CoCrMo. * indicates the mean difference is significant at p < 0.05.
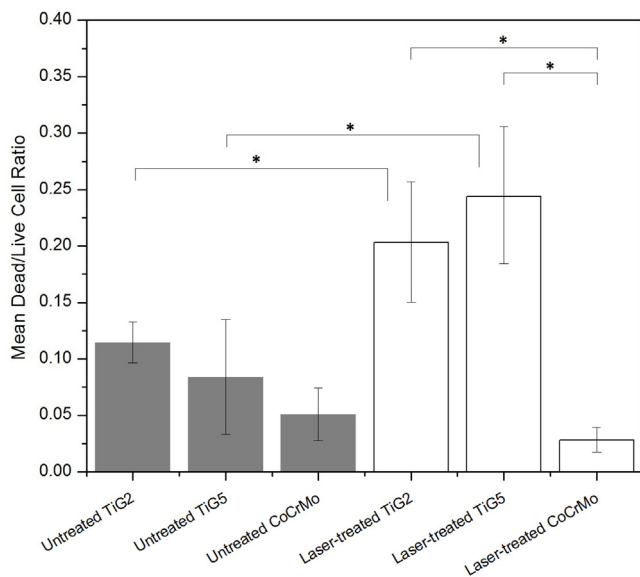
Fig. 9. Mean dead/live cell ratios (n = 10) with error bars (95% confident interval) for the two groups of samples: untreated and laser-treated samples. Within the group of untreated samples, no significant differences are observed. Within the group of laser-treated samples, no significant differences exist between the laser-treated TiG2 and TiG5, but significant differences are observed between the laser-treated TiG2 and CoCrMo as well as the laser-treated TiG5 and CoCrMo (p < 0.05). Comparing between the untreated and laser-treated samples, a statistically significant increment (p < 0.05) are observed with the laser-treated TiG2 and TiG5, respectively. No significant differences exist between the untreated and laser-treated CoCrMo. * indicates the mean difference is significant at p < 0.05.

a higher dead/live cell ratio than their untreated counterparts. The results are statistically significant at p < 0.05. It is important to note that although the mean dead/live cell ratio is higher for the laser-treated TiG5 than the laser-treated TiG2, their difference is not statistically significant, and thus, there is no statistical evidence to claim that the laser-treated TiG5 possesses stronger bactericidal effect than the laser-treated TiG2. However, it can still be concluded that the laser-treated TiG2 and TiG5 have a more efficacious bactericidal effect than their untreated counterparts. The laser-treated CoCrMo possesses a very weak bactericidal effect, as does the untreated CoCrMo.

3.8. SEM micrographs of biofilms

The SEM micrographs in Fig. 10 shows the morphology of *S. aureus* biofilms on the untreated (Fig. 10a, c and e) and laser-treated (Fig. 10b, d, and f) surfaces after 24 h culture. The SEM micrograph in Fig. 10a indicates that the untreated TiG2 surface is covered by a large number of adherent bacterial cells with evidence of biofilm formations, i.e. coccoid cells embedded in extracellular polymeric substances (EPS). Likewise, aggregates of coccoid cells embedded in EPS are found on the untreated TiG5 surface (Fig. 10c). Moreover, it appears that the biofilms on the untreated TiG2 and TiG5 preferably adhere on the pre-existing surface features, such as grooves from grinding. It appears that the untreated CoCrMo surface was almost completely covered by thick, confluent biofilms (Fig. 10e). In comparison, a significantly reduced amount of bacterial adherence was observed from the laser-treated TiG2 and TiG5 surfaces (Fig. 10b and d), with the number of adherent cells considerably reduced. The adherent cells on the laser-treated TiG2 and TiG5 surfaces show preferential adhesion on the surface micro-features, namely ripples and lamellae within the laser-treated areas. The biofilm on the laser-treated CoCrMo (Fig. 10f) is confluent in areas and more likely to adhere on the circular patterns along the laser tracks. The observations in the SEM micrographs are in good agreement with those in the fluorescence images and statistical analysis.

4. Discussion

The experimental results show that the laser-treated TiG2 and TiG5 exhibit notable antibacterial activities, namely higher resistance to bacterial attachment and colonisation (stronger on TiG2) and bactericidal effect (stronger on TiG5). In comparison, the laser-treatment of the CoCrMo had no obvious effect on either inhibiting the bacterial attachment and colonisation or killing the attached bacteria. The antibacterial activities of the Ti-based materials after laser treatment cannot be straightforwardly explained by the formation of TiN, given that whether or not the TiN itself exhibited the antibacterial properties is still controversial. Consequently, it is more appropriate to explain the antibacterial activities based on the (1) physiochemical (surface hydrophobicity), (2) chemical (oxide film composition, thickness and charge carrier properties) and (3) physical (surface roughness and topography) changes in the surfaces after laser treatment.

4.1. Physiochemical changes: surface hydrophobicity

Attachment of bacteria to a surface depends on a number of factors, such as Brownian movement, van der Waals forces, gravitational forces, electrostatic forces and hydrophobic interactions between the bacterial cell and the substratum. Bacterial attachment can be described by a two-stage process: an initial reversible attachment in the first step followed by an irreversible attachment in the second step [25]. Hydrophobic interactions are involved in the both steps and are considered to be an important factor in enabling the initial attachment of bacteria [26]. It is known

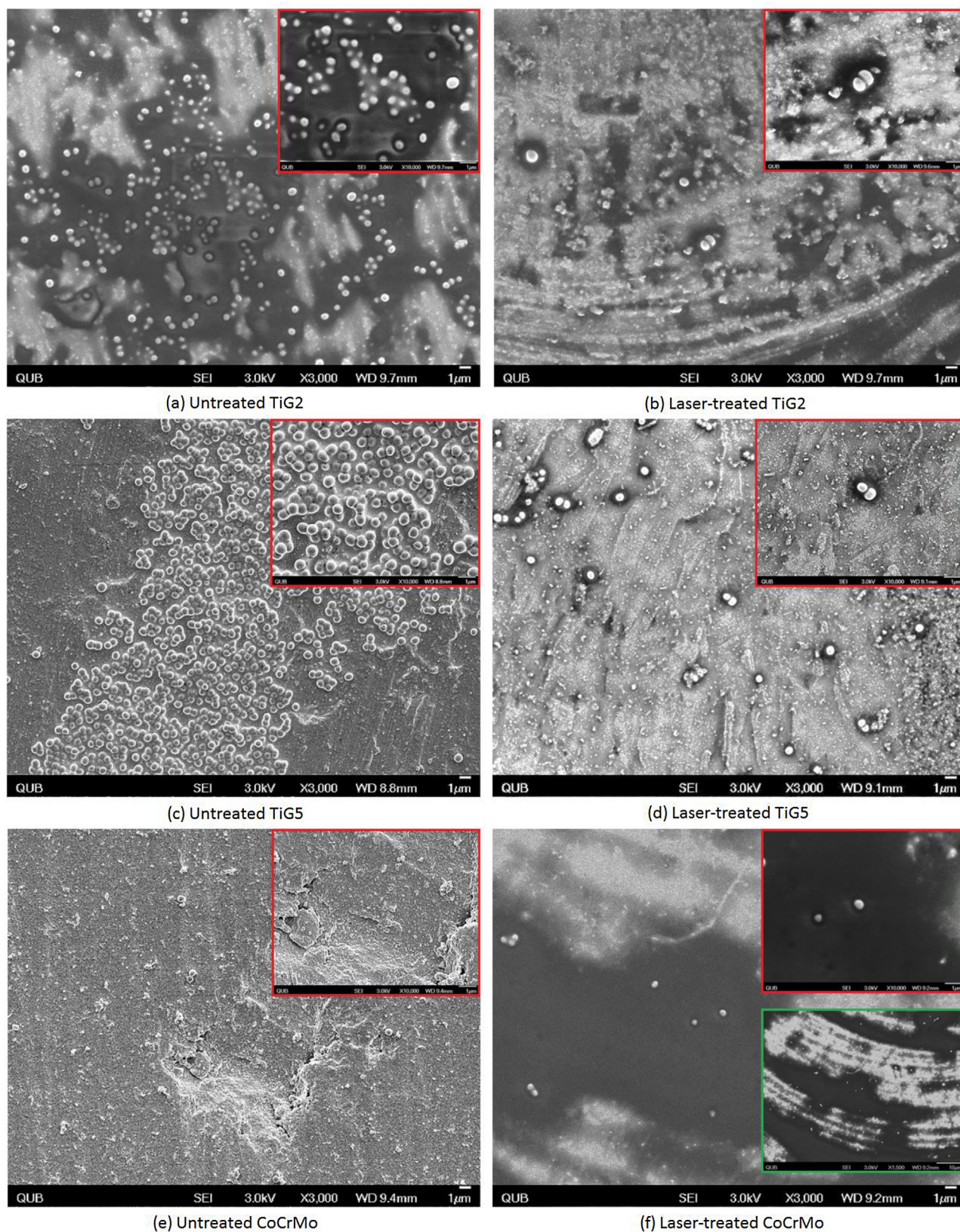**Fig. 10.** SEM micrographs for the untreated and laser-treated samples after 24 h of bacterial cell culture: TiG2 (a and b), TiG5 (c and d) and CoCrMo (e and f). The red-boxed insets in (a to f) show the higher magnification SEM images (10,000×) for different surfaces. The green-boxed inset in (f) is a lower magnification SEM image (1500×) showing the bacteria preferably adhere to the circular patterns of the laser tracks.

that more hydrophobic cells adhere more strongly to hydrophobic surfaces, whereas more hydrophilic cells adhere more strongly to hydrophilic surfaces [27]. *S. aureus* is typically hydrophobic [28]. The cell surface analysis performed by Mitik-Dineva et al. [29] indicated that *S. aureus* cells exhibited more hydrophobic characteristics (water contact angle of 72°) than *Escherichia coli and Pseudomonas aeruginosa* cells (water contact angle of 34° and 43°, respectively). The hydrophobic nature of *S. aureus* cells is attributable to the presence of highly negatively charged and hydrophobic teichoic and lipoteichoic acid (LTA) sites which are the main constituents of *S. aureus* cell walls [30,31]. As a consequence of the preference of hydrophobic cells for hydrophobic substrata, hydrophobic *S. aureus* has a lower tendency to adhere to hydrophilic surfaces. For instance, Hsieh and Timm [32] studied the relationship of substratum wettability and initial *S. aureus* adhesion to different polymer films, namely PTFE, PE, PP, PET, nylon 66, and acetate. They found that increasing *S. aureus* adhesion was correlated with decreasing surface water wettability (or higher water contact angle). The results of Mitik-Dineva et al. [29] showed that *S. aureus* was found to attach less than *E. coli* and *P. aeruginosa* to hydrophilic glass surfaces (water contact angle of 45°). Cunha et al. [5] reported that hydrophilic surfaces (water contact angles between 13° and 32°) created by laser treatment could reduce the adhesion of *S. aureus* on Grade 2 Ti alloy.

When analysing the samples in the present study, the CoCrMo surface after laser treatment remained hydrophobic, and thus, no reduction of bacterial attachment was observed. With regards to TiG2 and TiG5, the laser-treated samples are hydrophilic whilst those of the untreated are hydrophobic. Therefore, notably less bacterial attachment was found on laser-treated TiG2 and TiG5, i.e. the hydrophilic nature of the surfaces inhibited the attachment of hydrophobic *S. aureus* cells.

4.2. Chemical changes: oxide film composition, thickness and charge carrier properties

A thin oxide film is present on the outermost surfaces of all untreated samples. Such a naturally-formed oxide film is amorphous in structure and usually of few nm in thickness. The oxide film thickness is an important factor in relation to bacterial attachment as it directly influences the number of surface charge carriers in the oxide film, i.e. usually the higher the oxide film thickness, the smaller the number of charge carriers [33]. Surface charge carriers are responsible for the electrostatic interactions of bacteria with a surface. The number of charge carriers decreases in a thicker film due to inward diffusion into the bulk of the film [33]. As seen in the XPS spectrum, the oxide film on all the untreated samples is of variable thickness with some areas very thin, with metallic elements presents at or very near the surfaces. Further, excessive surface defects, such as Ti^{3+} point defects and oxygen vacancies which act as traps for charge carriers are present in the oxide film. Thus, there is substantial contribution from the surface defects, and the thin oxide film would behave as an *n*-type semiconductor. Accordingly, there is a relatively high proportion of charge carriers present at the surface of untreated samples, leading to ample bacterial attachment.

In comparison, the XPS spectra of the laser-treated samples indicate that the outermost surfaces are covered by a thicker film. The surface film is composed of nitride and oxides in laser-treated TiG2 and TiG5, whilst the film in laser-treated CoCrMo is composed of oxides. It has been reported that the laser-formed oxide film is more crystalline than the naturally-formed counterpart [15]. For laser-treated TiG2 and TiG5, their antibacterial activities can be ascribed to a chemical stabilization mechanism (as reported by Jeyachandran, et al. [13,14]) and to a film thickening effect. First, the laser-treated Ti surfaces attain chemical stability through the oxidation or nitridation of defect states in the surface film, i.e. oxidizing the metallic Ti into the TiO or TiO_2 and converting the surface defects: Ti^{3+} into the stable nitride TiN and sub-stoichiometric oxides Ti_2O_3. Consequently, the laser-treated surfaces are free from unsaturated bonds and immune to further reactions with bacteria. Second, although both the oxide and nitride are *n*-type semiconductors, a much thicker film was formed in the laser treatment (i.e. no metallic Ti signal seen in the XPS). The thicker film would indeed act as a strong barrier to electron transport from the substrate to the surface. So, the laser-treated Ti samples would have a lower capacity to donate electrons to the bacteria, and therefore less bacterial attachment is seen on the surfaces after laser treatment.

It is important to note that laser-treated TiG2 demonstrates a stronger antibacterial effect, in terms of bacterial attachment, than that of laser-treated TiG5. This is probably due to the combined effect of chemical composition and concentration of TiO_2 in the surface film. It has been reported that bacteria preferentially attach to areas rich in vanadium in titanium alloys [8]. Although no vanadium content can be detected from the TiG5 surface after laser-treatment, the vanadium in the substrate might still have the effect of encouraging bacterial attachment. Further, the surface film in laser-treated TiG2 has a higher concentration of TiO_2 than that of the laser-treated TiG5. As previously mentioned, the laser-formed oxide film is more crystalline in structure. It is known that crystalline TiO_2, particularly the Anatase phase, possesses a stronger antibacterial effect than amorphous TiO_2 [34]. The stronger resistance to bacterial attachment might be attributable to the higher concentration of crystalline TiO_2 in the surface film. It is interesting to note that laser-treated CoCrMo does not noticeably affect bacterial attachment, even though the oxide film is thickened and higher chemical stabilization is attained by complete oxidation of metallic Co and Cr. However, it is still inconclusive that the differences of bacterial attachment between CoCrMo and Ti-based alloys can be attributed to the chemical composition, and further investigations are required to study about this in greater detail.

4.3. Physical changes: surface roughness and topography

It is generally accepted that bacteria prefer to adhere on rougher surfaces since they offer a higher surface area for attachment while protecting the cells from unfavourable environmental disturbances such as shear forces [12]. Cunha et al. [5] have provided a concise summary of the influence of surface roughness on the microbial retention of *S. aureus*, and they have indicated that bacteria adhered preferentially to the surfaces with topographic features larger than the bacteria size (1–2 μm). The results of 2D roughness measurements indicate that all samples after laser treatment show a significant increase in the Ra value. However, an obvious reduction in bacterial attachment, instead of an increase, is observed for laser-treated TiG2 and TiG5 whereas laser-treated CoCrMo shows a comparable bacterial attachment with that of the untreated sample. No definite correlation exists between Ra and bacterial attachment in the present study. Likewise, the bactericidal effect of laser-treated TiG2 and TiG5 cannot be simply explained by the Ra value. To gain a deeper insight, kurtosis (Rku) and skewness (Rsk) were used to characterise the TiG2 and TiG5 surfaces after laser treatment. Two surfaces with similar Ra can show different Rku and Rsk values [24]. As seen in the AFM results, both laser-treated TiG2 and TiG5 possess higher skewness and kurtosis values than their untreated counterparts. This in turn indicates that the surfaces of laser-treated TiG2 and TiG5 are spikier (Rku > 3) with more peaks than troughs (Rsk > 0). The bactericidal effect is believed to be associated with the "spiky" surfaces in laser-treated TiG2 and TiG5, analogous to the bactericidal effect of the Cicada wings reported by Pogodin et al. [11], wherein bacteria/material interactions adsorb the bacterial cell tightly onto the material surface,

allowing for the nanostructures on the Cicada wing to pierce the bacterial cell membrane, leading to cell rupture and lysis. The spiky surfaces are the consequences of the laser-induced nano-features as seen in the AFM 3D image. It is notable that both laser-treated TiG2 and TiG5 have a positive skewness value but the latter has a higher kurtosis value (Rku of 3.04 versus 3.11), indicating that the surface of laser-treated TiG5 is spikier. This may also explain why the laser-treated TiG5 possesses stronger bactericidal effect.

In summary, the attachment of *S. aureus* cells to the metallic surfaces studied, namely TiG2, TiG5 and CoCrMo, is driven by the surface hydrophobicity and surface chemistry rather than surface roughness whilst the bactericidal effect is likely to be determined by the surface topography (or surface spikiness).

5. Conclusions

Three different orthopaedic implant materials, namely CP Ti, Ti6Al4V and CoCrMo alloys, were laser-treated by a fibre laser with a 1064 nm wavelength in a nitrogen shielding environment. The antibacterial properties of the untreated and laser-treated samples were compared and analysed. The following conclusions are reached:

1. The surface roughness of all materials was increased significantly after laser treatment. Laser-treated CP Ti and Ti6Al4V tended to have a spiky surface with more peaks than troughs;
2. The surface hydrophobicity of CP Ti and Ti6Al4V was greatly reduced after laser treatment but no change was observed on laser-treated CoCrMo;
3. Both nitrides (TiN) and oxides (TiO_2) were present on the laser-treated CP Ti and Ti6Al4V surfaces, however, only oxides (CoO and Cr_2O_3) were found from the laser-treated CoCrMo. The surface oxides of all laser-treated materials were free from metallic components and their thicknesses were increased by the treatment.
4. The bacterial adhesion of *S. aureus* cells on laser-treated CP Ti and Ti6Al4V surfaces was reduced significantly, and a bactericidal effect was seen on these surfaces. No reduction of bacterial adhesion and bactericidal effect were observed for laser-treated CoCrMo.

In conclusion, laser treatment of CP Ti and Ti6Al4V surfaces using a fibre laser at 1064 nm in the nitrogen environment was found to promote their antibacterial properties. These antibacterial properties resulted from both reduced bacterial adhesion and to a bactericidal effect. These effects on the laser treated CP Ti and Ti6Al4V surfaces were attributed to the combined effects of reduced hydrophobicity, the presence of thicker and stable nitride and oxide films, and to presence of laser-induced nano-features.

Acknowledgements

References

[1] Grand View Research Inc., Orthopedic implants market analysis, by application (spinal fusion, long bone, foot & ankle, craniomaxillofacial, joint replacement, dental), and segment forecasts to 2024 (market research report code: GVR-1-68038-020-0). http://www.grandviewresearch.com/industry-analysis/orthopedic-implants-market/, 2016 (Accessed 30 October 2016).

[2] M.A. Getzlaf, E.A. Lewallen, H.M. Kremers, D.L. Jones, C.A. Bonin, A. Dudakovic, R. Thaler, R.C. Cohen, D.G. Lewallen, A.J. van Wijnen, Multi-disciplinary antimicrobial strategies for improving orthopaedic implants to prevent prosthetic joint infections in hip and knee, J. Orthop. Res. 34 (2016) 177–186.

[3] J.T. Kempthorne, R. Ailabouni, S. Raniga, D. Hammer, G. Hooper, Infection in aseptic joint loosening and the diagnostic role of implant sonication, BioMed Res. Int. 2015 (2015) 946215.

[4] H. Havard, J. Miles, Biofilm and orthopaedic implant infection, J. Orthop. Trauma 3 (2015) 54–57.

[5] A. Cunha, A.M. Elie, L. Plawinski, A.P. Serro, A.M.B. do Rego, A. Almeida, M.C. Urdaci, M.C. Durrieu, R. Vilar, Femtosecond laser surface texturing of titanium as a method to reduce the adhesion of staphylococcus aureus and biofilm formation, App. Surf. Sci. 360 (2016) 485–493.

[6] M. Ribeiro, F.J. Monteiro, M.P. Ferraz, Infection of orthopedic implants with emphasis on bacterial adhesion process and techniques used in studying bacterial-material interactions, Biomatter 2 (2012) 176–194.

[7] A. Fan, H. Zhang, Y. Ma, X. Zhang, J. Zhang, B. Tang, Bacteria adherence properties of nitrided layer on Ti6Al4V by the plasma nitriding technique, J. Wuhan Univ. Technol.- Mater. Sci. Ed. 28 (2013) 1223–1226.

[8] M.I. Sarró, D.A. Morenoa, C. Ranninger, E. King, J. Ruiz, Influence of gas nitriding of Ti6Al4V alloy at high temperature on the adhesion of Staphylococcus aureus, Surf. Coat. Tech. 201 (2006) 2807–2812.

[9] A. Pagedar, J. Singh, V.K. Batish, Surface hydrophobicity, nutritional contents affect staphylococcus aureus biofilms and temperature influences its survival in preformed biofilms, J. Basic Microbiol. 50 (2010) S98–S106.

[10] A.M. Gallardo-Moreno, M.A. Pacha-Olivenza, L. Saldaña, In vitro biocompatibility and bacterial adhesion of physico-chemically modified Ti6Al4V surface by means of UV irradiation, Acta Biomater. 5 (2009) 181–192.

[11] S. Pogodin, J. Hasan, V.A. Baulin, H.K. Webb, V.K. Truong, T.H. Phong Nguyen, V. Boshkovikj, C.J. Fluke, G.S. Watson, J.A. Watson, R.J. Crawford, E.P. Ivanova, Biophysical model of bacterial cell interactions with nanopatterned Cicada wing surfaces, Biophys. J. 104 (2013) 835–840.

[12] L.C. Hsu, J. Fang, D.A. Borca-Tasciu, R.W. Worobo, C.I. Moraru, Effect of micro- and nanoscale topography on the adhesion of bacterial cells to solid surfaces, Appl. Environ. Microbiol. 79 (2013) 2703–2712.

[13] Y.L. Jeyachandran, S.K. Narayandass, D. Mangalaraj, C.Y. Bao, W. Lib, Y.M. Liao, C.L. Zhang, L.Y. Xiao, W.C. Chen, A study on bacterial attachment on titanium and hydroxyapatite based films, Surf. Coat. Tech. 201 (2006) 3462–3474.

[14] Y.L. Jeyachandran, S. Venkatachalama, B. Karunagarana, Bacterial adhesion studies on titanium, titanium nitride and modified hydroxyapatite thin films, Mater. Sci. Eng. C. 27 (2007) 35–41.

[15] C.W. Chan, S. Lee, G. Smith, G. Sarri, C.H. Ng, A.S. Sharba, H.C. Man, Enhancement of wear and corrosion resistance of beta titanium alloy by laser gas alloying with nitrogen, App. Surf. Sci. 367 (2016) 80–90.

[16] J. Zhou, C. Gao, P. Feng, T. Xiao, C. Shuai, S. Peng, Calcium sulfate bone scaffolds with controllable porous structure by selective laser sintering, J. Porous Mater. 22 (2015) 1171–1178.

[17] C. Shuai, J. Zhou, D. Gao, C. Gao, P. Feng, S. Peng, Functionalization of calcium sulfate/bioglass scaffolds with zinc oxide whisker, Molecules 21 (2016) 378.

[18] T. Kawano, W. Prananingrum, Y. Ishida, T. Goto, Y. Naito, M. Watanabe, Y. Tomotake, T. Ichikawa, Blue-violet laser modification of titania treated titanium: antibacterial and osteo-inductive effects, PLoS One 8 (2013) e84327.

[19] A. Gillett, D. Waugh, J. Lawrence, M. Swainson, R. Dixon, Laser surface modification for the prevention of biofouling by infection causing Escherichia Coli, J. Laser App. 28 (2016) 022503.

[20] A.F. Chen, C.B. Wessel, N. Rao, Staphylococcus aureus screening and decolonization in orthopaedic surgery and reduction of surgical site infections, Clin. Orthop. Relat. Res. 471 (2013) 2383–2399.

[21] C.W. Chan, S. Lee, G.C Smith, C. Donaghy, Fibre laser nitriding of titanium and its alloy in open atmosphere for orthopaedic implant applications: Investigations on surface quality, microstructure and tribological properties, Surf. Coat. Tech. 309 (2017) 628–640.

[22] I. Horcas, R. Fernandez, J.M. Gomez-Rodriguez, J. Colchero, J. Gómez-Herrero, A.M. Baro, A software for scanning probe microscopy and a tool for nanotechnology, Rev. Sci. Instrum. 78 (2007) 013705.

[23] W.J. Suder, S.W. Williams, Investigation of the effects of basic laser material interaction parameters in laser welding, J. Laser Appl. 24 (2012) 032009.

[24] M.J. Giraldez, C.G. Resua, M. Lira, M.E. Oliveira, B. Magariños, A.E. Toranzo, E. Yebra-Pimentel, Contact lens hydrophobicity and roughness effects on bacterial adhesion, Optom. Vis. Sci. 87 (2010) E426–E431.

[25] R.M. Goulter, I.R. Gentle, G.A. Dykes, Issues in determining factors influencing bacterial attachment: a review using the attachment of Escherichia Coli to abiotic surfaces as an example, Lett. Appl. Microbiol. 49 (2009) 1–7.

[26] M. Rosenberg, S. Kjelleberg, Hydrophobic interactions: role in bacterial adhesion, in: K. Marshall (Ed.), Advances in Microbial Ecology, vol. 9, Springer Science & Business Media, New York, 2013, pp. p353–383.

[27] A. Krasowska, K. Sigle, How microorganisms use hydrophobicity and what does this mean for human needs, Front. Cell. Infect. Microbiol 4 (2014) 1–7.

[28] F. Reifsteck, S. Wee, B.J. Wilkinson, Hydrophobicity-hydrophilicity of Staphylococci, J. Med. Microbiol. 24 (1987) 65–73.

[29] N. Mitik-Dineva, J. Wang, V.K. Truong, P. Stoddart, F. Malherbe, R.J. Crawford, E.P. Ivanova, Escherichia coli, Pseudomonas aeruginosa, and Staphylococcus aureus attachment patterns on glass surfaces with nanoscale roughness, Curr. Microbiol. 58 (2009) 268–273.

[30] P. Canepari, M. Boaretti, M.M. Lleo, G. Satta, Lipoteichoic acid as a new target for activity of antibiotics: mode of action of daptomycin (ly146032), Antimicrob. Agents Chemother. 34 (1990) 1220–1226.

[31] M. Gross, S.E. Cramton, F. Götz, A. Peschel, Key role of teichoic acid net charge in *Staphylococcus aureus* colonization of artificial surfaces, Infect. Immun. 69 (2001) 3423–3426.

[32] Y.L. Hsieh, D.A. Timm, Relationship of substratum wettability measurements and initial *Staphylococcus aureus* adhesion to films and fabrics, J. Colloid Interface Sci. 123 (1988) 275–286.

[33] Y.L. Jeyachandran, S.K. Narayandass, The effect of thickness of titanium nitride coatings on bacterial adhesion, Trends Biomater. Artif. Organs 24 (2010) 90–93.

[34] L. Visai, L. De Nardo, C. Punta, L. Melone, A. Cigada, M. Imbriani, C.R. Arciola, Titanium oxide antibacterial surfaces in biomedical devices, Int. J. Artif. Organs 9 (2011) 929–946.